# Analysis of voltage stability characterization of radial distribution grids with high penetration of distributed energy resources

*Todor* Todorov[1*], *Ivaylo* Stoyanov[2], and *Teodora* Hristova[2,3]

[1]AC DC Energy Ltd, 1000 Sofia, Bulgaria
[2]University of Ruse, Department of Electrical Power Engineering, 7004 Ruse, Bulgaria
[3]University of Mining and Geology "St. Ivan Rilski", Department of Electricity and Automation, 1700 Sofia, Bulgaria

**Abstract.** The high penetration of distributed energy resources (DER) in radial distribution grids shifts the voltage stability from low to high voltage. This paper presents an analytical framework for comparing voltage changes across different regimes. Six classical voltage stability indices (VSI, VSF, Lmn, FVSI, VQI, and L-index) are compared for the impact of photovoltaic, wind, and battery energy storage systems (BESS) on the IEEE 33-bus radial distribution test system. In the article, three scenarios of DER penetration - low (0–30%), moderate (30–70%), high (70–120%), and very high (>120% of peak load) are studied for the subsequent determination of energy saving and grid balancing regimes. The derived closed-form sensitivity factors ∂, VSI/$\partial P_{DER}$ and $\partial VSI/\partial Q_{DER}$, for radial branches with net reverse power flow, are obtained, and inverter control modes with Q(U) Volt-Var and P(U) Volt-Watt are suggested, compatible with EN 50549/IEEE 1547. The L-index for determining the optimal power flow (OPF) is analyzed. The proposed framework provides distribution system operators with an analytically sound, computationally efficient methodology for integrating DER.

## 1 Introduction

The accelerating deployment of inverter-based distributed energy resources, such as rooftop photovoltaic (PV) systems, small wind turbines, and battery energy storage systems (BESS), induces an imbalance in the energy grid. They fundamentally alter the power-flow patterns in radial distribution grids. In conventional passive operation, power flows unidirectionally from the substation to the load buses, and voltage stability analysis is limited to ensuring that the load buses remain above the collapse limit defined by the peak of the P-U curve [1, 2]. However, with increasing DER penetration, net power injection into the load buses can reverse the direction of branch flows [3], raising bus voltages and introducing an overvoltage-limited mode of operation that coexists with the classical undervoltage collapse limit [4].

* Corresponding author: tn_todorov@abv.bg

The voltage stability indices (VSI) are efficient scalar metrics for quantifying the proximity to voltage instability without the need for power flow continuation or iterative eigenvalue analysis [5]. Voltage stability indices (VSIs) are efficient scalar metrics for quantifying proximity to voltage instability without requiring continuation power flow or iterative eigenvalue analysis [5].

Many studies use a single index as a post hoc evaluation metric after DER layout optimization, rather than comparing multiple indices under identical conditions. In [6], VSI is used as a preliminary candidate bus selector within the Multi-Layer Particle Swarm Optimization (MLPSO) framework of an IEEE 33-bus system, and recent metaheuristic studies use NLSI, VSI, or PSI individually [7]. To the best of the authors' knowledge, no systematic side-by-side comparison of six or more classical indices has been reported for common DER scenarios.

With the penetration of DER, a transition from undervoltage to overvoltage operation is observed. The quantitative impact of modern inverter control modes — in particular, the droop functions Q(U) Volt-Var and P(U) Volt-Watt required by EN 50549-1:2019 and IEEE Std 1547-2018 — on canonical analytical VSIs remains largely unexplored. In [8], the L-index was recently combined with digital twin-driven Volt/VAR optimization. They demonstrated a 76.5% improvement in the static voltage stability margin. Index families and mode transitions according to penetration are not analyzed.

The rest of this paper is organized as follows. Section II presents the analytical framework, the two-bus equivalent model, the derivation of the P-U and Q-U curves, and the six index definitions. Section III derives the sensitivity coefficients. The formulation of the OPF with stability constraints is in Section IV, and Section V presents results from a case study of an IEEE 33-bus system.

# 2 Analytical foundation

## 2.1 Voltage equation for a radial branch

Consider a single radial feeder segment from the sending-end bus i (voltage $U_i$) to receiving-end bus j (voltage $U_j$) through a branch with impedance $Z = R + jX$, delivering power $S_J = P_j + iQ_j$. The receiving-end voltage satisfies [8]:

$$U_j^2 = U_i^2 - 2(R \cdot P_j + X \cdot Q_j) - \frac{\left(R^2+X^2)(P_j^2+Q_j^2\right)}{U_j^2} \tag{1}$$

Rearranging (1) as a quadratic in $V = U_j^2$:

$$V^2 - \left[U_i^2 - 2\left(R \cdot P_j + X \cdot Q_j\right)\right]V + (R^2 + X^2)\left(P_j^2 + Q_j^2\right) = 0 \tag{2}$$

The discriminant is:

$$\mathcal{D} = \left[U_i^2 - 2(R \cdot P_j + X \cdot Q_j)\right]^2 - 4(R^2 + X^2)(P_j^2 + Q_j^2) \tag{3}$$

A real, positive voltage solution exists if and only if $\mathcal{D} \geq 0$. The voltage stability boundary (nose point of the P-U curve) occurs at $\mathcal{D} = 0$.

## 2.2 Maximum deliverable power

For a purely resistive branch ($X = 0$, relevant to LV cables where $R/X \gg 1$):

$$\mathcal{D}P_{j,\max} = \frac{U_i^2}{4R}, \quad (4)$$

at a receiving-end voltage of $U_j = {U_j}/{\sqrt{2}} \approx 0{,}707U_i$. For the general case with load power factor cos φ (where $Q_j = P_j tan\varphi\ P_j$):

$$\mathcal{D}P_{j,\max} = \frac{U_i^2}{2|Z|} \cdot \frac{1}{1+\cos(\alpha-\varphi)}, \quad (5)$$

where $\alpha$ is the branch impedance angle. Maximum power transfer occurs when $\varphi = \alpha$, yielding $P_{\mathrm{j,max,abs}} = U_i^2/(4|Z|)$.

### 2.3 Voltage stability margin

The voltage stability margin (VSM) at an operating point is:

$$\mathrm{VSM} = \frac{P_{j,\max} - P_{j,\mathrm{op}}}{P_{j,\max}} \times 100\% \quad (6)$$

Distribution grids typically operate with VSM > 30–50%, but DER-induced reverse power flows can significantly alter these margins.

### 2.4 Voltage stability indices

Six indices are employed in this study, selected for their physical interpretability, computational efficiency, and suitability for radial grids with bidirectional power flow.

The criteria used are:
- Voltage Stability Flow VSF;
- Voltage Stability Margin VSM;
- Voltage Stability Indices $\mathrm{VSI}_j$;
- L-index;
- Voltage Quality Index – $\mathrm{VQI}_j$;
- Fast Voltage Stability Index FVSI.

FVSI requires only readily available power flow data (no angle computations), making it computationally efficient for large grids.

Table 1 summarizes the six indices, their stability criteria, and computational requirements.

**Table 1.** Summary of Voltage Stability Indices.

| Index | Type | Stable range | Critical value | Computational requirements |
|---|---|---|---|---|
| VSI | Branch | VSI > 0 | VSI = 0 | Low |
| VSF | Bus | VSF > 0.707 | VSF = 0.707 | Very low |
| $L_{mn}$ | Branch | $L_{mn}$< 1 | $L_{mn}$= 1 | Low |
| FVSI | Branch | FVSI < 1 | FVSI = 1 | Very low |
| VQI | Bus/Branch | VQI < 1 | VQI = 1 | Low |
| L-index | Bus | L < 1 | L = 1 | Moderate |

https://doi.org/10.1051/e3sconf/202672703004

## 3 Framework and sensitivity analysis

### 3.1 Net power injection with DER

The presence of DER at bus j modifies the net power injection from pure load ($P_L$, to $-Q_L$) to:

$$P_j^{\text{net}} = P_{\text{DER},j} - P_{L,j}; \tag{7}$$

$$Q_j^{\text{net}} = Q_{\text{DER},j} - Q_{L,j}. \tag{8}$$

The branch power flow toward bus j in a radial grid becomes:

$$P_{\text{br}} = \sum_{k\in\mathcal{D}(j)} P_{L,k} - P_{\text{DER},j} + P_{\text{loss,ds}}; \tag{9}$$

$$Q_{\text{br}} = \sum_{k\in\mathcal{D}(j)} Q_{L,k} - Q_{\text{DER},j} + Q_{\text{loss,ds}}, \tag{10}$$

where $\mathcal{D}(j)$ denotes the set of buses downstream of branch (i, j). Substituting into (7):

$$\text{VSI}_j^{\text{DER}} = U_i^4 - 4(P_{\text{br}}X_{ij} - Q_{\text{br}}R_{ij})^2 - 4(P_{\text{br}}R_{ij} + Q_{\text{br}}X_{ij})U_i^2 \tag{11}$$

The Voltage Stability Improvement Index (VSII) quantifies the relative change:

$$\text{VSII}_j = \frac{\text{VSI}_j^{\text{DER}} - \text{VSI}_j^{\text{base}}}{\text{VSI}_j^{\text{base}}} \times 100\% \tag{12}$$

### 3.2 Voltage stability

As DER penetration increases from 0% to over 100% of peak load, the voltage stability indices go through three distinct phases. Let $\lambda = P_{DER,total}/P_{load}$, peak denote the penetration coefficient (Figure 1).

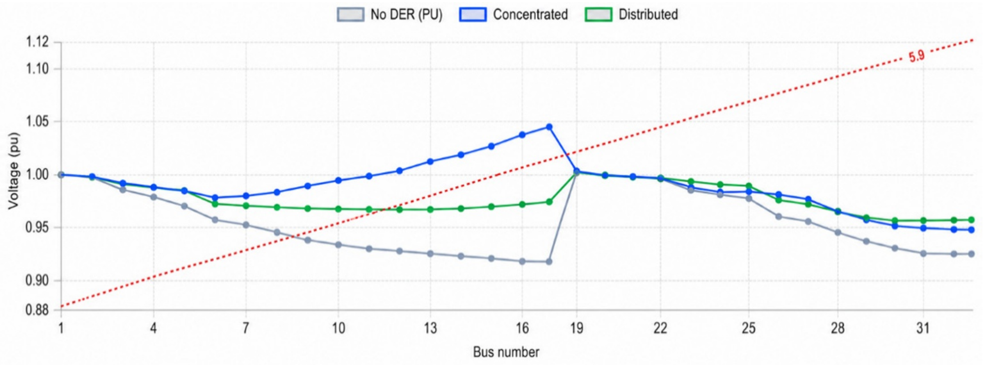


**Fig. 1.** Influence of the DER penetration and voltage stability indices.

Phase 1 of a low penetration ($0 < \lambda \leq 0.30$). All VSI values increase monotonically. The weakest bus is strengthened. The parameters L-index, power per voltage, and reactive losses decrease. All six indices studied have improved stability. This phase is clearly beneficial.

Phase 2 of a moderate penetration ($0.30 < \lambda \leq 0.70$). VSI values continue to improve, but with diminishing marginal returns. Losses and the L-index reach a minimum, and the rate of DER improvement slows. In this case, the voltage deviation is close to zero and to the L-index of the dependence ($P_{DER} \approx P_L$), the local VSI approaches its maximum.

Phase 2 — Moderate penetration (0.30 < λ ≤ 0.70). VSI values continue to improve, but with diminishing marginal returns. System losses and the L-index reach their minimum values, and the incremental stability benefit of additional DER capacity decreases. The local VSI reaches its maximum when the voltage deviation approaches zero, i.e., when the bus voltage is close to nominal and the operating point is constrained neither by undervoltage nor by overvoltage. This condition typically occurs when local DER generation approximately matches local load demand (PDER ≈ PL), minimizing the net active power flow through the feeder section.

Phase 3 of a high penetration (0.70 < λ ≤ 1.20). This is a borderline case for λ, ranging from 2 to 3, and control is required to avoid the transition from undervoltage to overvoltage at the minimum DER. In branches with DER, it increases close to the standard limit, and reverse power flow and reduced VSI are measured if the limit is narrowed ($U_{max} = 1.10$ p.u. according to EN 50160).

Phase 4 of a very high penetration (λ > 1.20). Reverse power flows and overvoltages due to reactive power generation by the lagging-mode inverter (saturation Q(U)) and active power generation by the inverter are observed. The instability is caused by the interaction between the source's equivalent impedance and the inverter's output impedance.

The presented analysis for the three considered phases depends on the grid topology, R/X ratio, load distribution, and the location of the DER. However, the qualitative progression is universal for radial feeders, and the limiting values can be calculated for any given grid by observing changes in the sign of the branch flows and the inflection points of the VSI curves. For this purpose, the crossover λ* is considered as the value at which the minimum bus voltage margin (distance to $U_{min}$ =0.90 p.u.) is equal to the minimum overvoltage margin (distance to $U_{max}$ = 1.10 p.u.) of the DER bus:

$$\lambda^{*}: \min_{j} (U_j - U_{\min}) = \min_{k} (U_{\max} - U_k), k \in \mathcal{N}_{\mathrm{DER}} \tag{13}$$

$$R/X > \lambda^{*} \tag{14}$$

Below λ*, undervoltage is the coupling constraint; above λ*, overvoltage is coupled to undervoltage. This crossover is observed across all six indices, confirming its physical (non-index-specific) origin.

### 3.3 Analytical sensitivity factors

The sensitivity of VSI at bus j to active power injection by DER at bus m is:

$$\sigma_{P,jm} = \frac{\partial \mathrm{VSI}_j}{\partial P_{\mathrm{DER},m}}. \tag{15}$$

From eq. (11), differentiating with respect to $P_{DER}$,m:

$$\sigma_{P,jm} = -4 \cdot 2(P_{\mathrm{br}}X - Q_{\mathrm{br}}R)(+X)\frac{\partial P_{\mathrm{br}}}{\partial P_{\mathrm{DER},m}} - 4U_i^2 R \frac{\partial P_{\mathrm{br}}}{\partial P_{\mathrm{DER},m}}. \tag{16}$$

For DER on the same feeder path (bus m upstream of or at bus j) as $\partial P_{\mathrm{br}}/\partial P_{\mathrm{DER},m} = -1$ (DER reduces branch flow by its full output). For a DER on a different lateral branch, it is valid. $\partial P_{\mathrm{br}}/\partial P_{\mathrm{DER},m} = 0$ (no direct effect). Substituting $\partial P_{\mathrm{br}}/\partial P_{\mathrm{DER},m} = -1$:

$$\sigma_{P,jm} = 8(P_{\mathrm{br}}X - Q_{\mathrm{br}}R)X + 4U_i^2 R. \tag{17}$$

The analogous reactive power sensitivity is:

$$\sigma_{Q,jm} = \frac{\partial \mathrm{VSI}_j}{\partial Q_{\mathrm{DER},m}} = [8(P_{\mathrm{br}}X - Q_{\mathrm{br}}R)R - 4U_i^2 X)](-1) \tag{18}$$

or

$$-8(P_{\mathrm{br}}X - Q_{\mathrm{br}}R)R + 4U_i^2X)].$$

This is when we have net injection from DER.

$$\sigma_{Q,jm} = \frac{\partial \mathrm{VSI}_j}{\partial Q_{\mathrm{DER},m}} = 4\mathrm{U}_i^2X - 8R(P_{br}X - Q_{br}R)$$

These sensitivities have three important properties (Figure 2).

$\sigma_{P,jm} > 0$ when the branch carries direct power flow $P_{Br} > 0$ and improved stability is observed in phases 1 and 2.

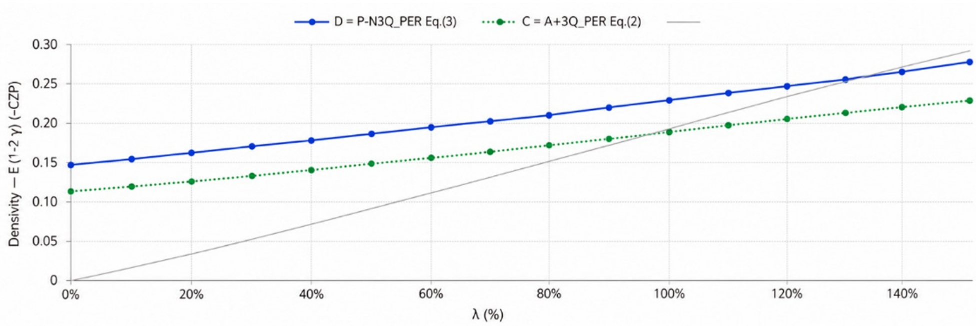


**Fig. 2.** The sensitivity of VSI at bus j to active power injection by DER.

With active power approaching zero and the transition from phase 2 to 3, $\sigma_{P,jm}$ approaches $4U_i^2R - 8Q_{br}RX$, depending on the reactive flow.

With reactance approaching zero, $\sigma_{P,jm} \to 4U_i^2R$. Resistive branches are observed in low-voltage (LV) grids. Stability increases before reaching overvoltage because VSI always improves with increasing DER. Analogous sensitivity expressions can be obtained for FVSI and $L_{mn}$ with respect to $P_{DER}$and $Q_{DER}$, which leads to:

$$\frac{\partial L_{mn}}{\partial Q_{\mathrm{DER},m}} = -\frac{4X_{mn}}{[U_m \sin(\theta_{mn} - \delta_m)]^2} \tag{19}$$

These closed-form sensitivities enable rapid, linearized assessment of how changes in DER dispatch affect stability margins without resolving the full power flow, making them suitable for real-time dispatch applications.

### 3.4 Impact of inverter control modes

Unity power factor (cos φ = 1, $Q_{DER} = 0$ provides only active power, and reactive power is supplied by the circuit input. There is no reactive power support for voltage stability.

Q(U) Volt-Var control (according to EN 50549 / IEEE 1547). The inverter dynamically regulates the output reactive power as a function of the terminal voltage.

In case of overvoltage (U > $U_3$= 1.02 p.u.), $Q_{DER} < 0$ (Lagging mode), the voltage rise must be reduced, and during under voltage (U < $U_2$= 0.98 p.u.), the voltage rise must be increased. If $Q_{DER} > 0$ is the generating mode, the voltage stability in phases 1 and 2 is maintained (Figure 3).

P(U) Volt-watt control. When the bus voltage exceeds a threshold (U > $U_{P,start}$, typically 1.06–1.08 p.u.), the inverter linearly limits the active output power.

Q(U) provides a self-regulating effect when the index improvement is largest precisely when and where it is most needed at the buses experiencing the greatest voltage deviation.

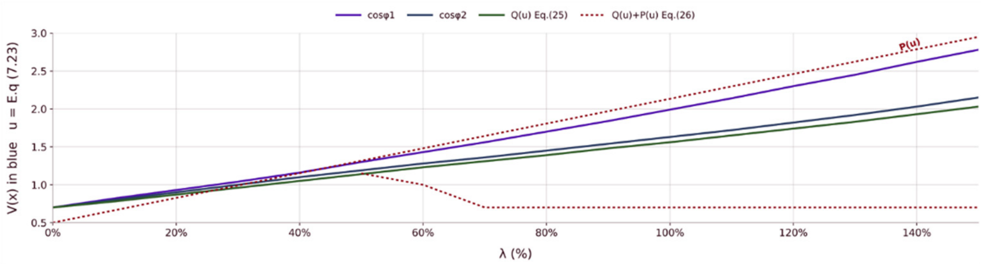


**Fig. 3.** The improvement in VSI due to Q(U) in the buses with the highest voltage deviation.

3) P(U) Volt-Watt control. When bus voltage exceeds a threshold (U > $U_{P,\text{start}}$, typically 1.06–1.08 p.u.), the inverter curtails active power output linearly:

$$P_{\text{DER}}(U) = \begin{cases} P_{\text{avail}} & U \leq U_{P,\text{start}} \\ P_{\text{avail}} \cdot \frac{U_{P,\text{stop}} - U}{U_{P,\text{stop}} - U_{P,\text{start}}} & U_{P,\text{start}} < U < U_{P,\text{stop}} \\ 0 & U \geq U_{P,\text{stop}} \end{cases} \tag{20}$$

P(U) curtailment prevents overvoltage but reduces energy yield. It does not improve the classical undervoltage stability margin, but rather, it constrains the operating regime to prevent entry into Phase 4.

### 3.5 Impact of battery energy storage systems

Battery energy storage systems (BESS) can modify and regulate the net injection at bus j:

$$P_j^{\text{net}} = P_{\text{DER},j} + P_{\text{BESS},j} - P_{L,j}, \tag{21}$$

where $P_{BESS} > 0$ during discharge and improved stability from power generation, or $P_{BESS} <$ 0 during low load charging, Lagging DER, and reducing reverse flow. BESS effectively extends the range of phases 1 and 2 and delays the start of phases 3 and 4 by absorbing excess generation. The increase in hosting capacity due to BESS is:

$$\Delta\text{HC}_{\text{BESS}} = \text{HC}_{\text{with BESS}} - \text{HC}_{\text{without BESS}} \tag{22}$$

P(U) Volt-watt control (Figure 4) is recommended when the bus voltage exceeds a threshold (U > $U_{P,\text{start}}$, typically 1.06–1.08 p.u.), the inverter linearly limits the active output power.

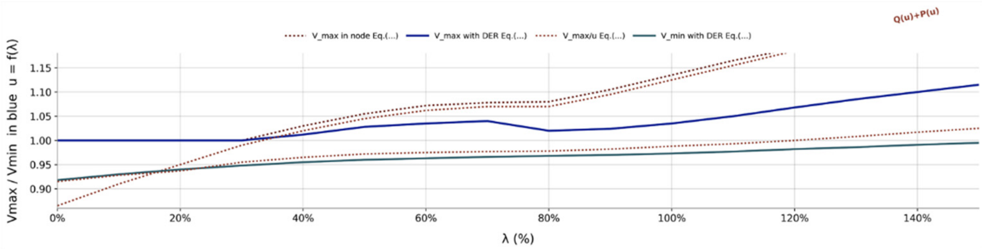


**Fig. 4.** Impact of battery energy storage systems on VSI.

### 3.6 Optimal power flow Formulation with voltage stability constraints

The optimal power flow equation with embedded voltage stability constraints takes the form:

$$\min_{x,u} f(x,u) \tag{23}$$

subject to:

$$g(x,u) = 0\text{(power flow equations)}; \tag{24}$$

$$U_{\min} \leq U_k \leq U_{\max} \forall k \in \mathcal{N}; \tag{25}$$

$$I_l \leq I_{l,\max} \quad \forall l \in \mathcal{B}; \tag{26}$$

$$\mathrm{VSI}_j \geq \mathrm{VSI}_{\min} \forall j \in \mathcal{N}_L; \tag{27}$$

$$L_j \leq L_{\max} \forall j \in \mathcal{N}_L, \tag{28}$$

where x is the state vector (bus voltages and angles), u is the control vector (DER active and reactive power outputs, OLTC tap positions), and f is the objective function (loss minimization, voltage deviation minimization, or a weighted combination). Equations (27)–(28) ensure that the optimized operating point remains sufficiently far from voltage collapse, even when the voltage magnitudes are within the statutory ±10% range. For stability, VSI minimum (20–30%), $L_{max}$ (0.7–0.8) is maintained within a 20–30% margin to the collapse point.

A procedure for placing DER at OPF with stability constraints is proposed:

• Step 1: Solve the base-case power flow without DER. Calculate the VSI for all buses and identify the weakest bus as j* = arg min_j VSI_j.

• Step 2: Gradually increase the DER capacity at bus j* and re-solve the power flow at each increment. For each step, record the DER capacity at which one of the following limits is reached: the target VSI threshold, the maximum voltage limit Umax = 1.10 p.u., or the thermal limit of any branch.

• Step 3: Determine the maximum allowable DER capacity at bus j* as the minimum of the limiting capacities identified in Step 2. For end-of-feeder locations, this limit is typically governed by overvoltage.

• Step 4: Repeat the procedure for additional candidate DER buses, recalculating the voltage stability indices after each placement.

• The sensitivity factors derived in (15)–(16) allow constraints (27)–(28) to be linearized around the current operating point. This enables the use of sequential linear programming or interior-point methods, improving computational efficiency.

# 4 Case study: IEEE 33-bus system

## 4.1 Test system and scenarios

The IEEE 33-bus radial distribution test system is used as a benchmark. The system consists of 33 buses and 32 branches, with a total active load of 3.715 MW and a reactive load of 2.300 Mvar in the base case. The substation voltage is 12.66 kV.

The DER penetration is parametrically increased from 0% to 150% of the peak load in 10% increments. Three DER deployment strategies are tested:

• concentrated in the weakest bus (Bus 18);
• distributed in three weak buses (Buses 18, 33, 25);
• evenly distributed in all load buses.

Three DER types are modeled: PV (unity power factor), wind (lagging power factor of 0.85), and PV+wind (mixed power factor). The BESS is sized at 20% of the DER capacity.

Three inverter control modes are compared at cos φ=1, cos φ = 0.95 (absorbing), Q(U) Volt-Var according to EN 50549, and combined Q(U) + P(U). The Q(U) characteristic uses a deadband of 0.98–1.02 p.u. with a maximum Q = ±0.4 p.u. of the rated power. The P(U) characteristic uses $U_{P,\mathrm{start}}$ = 1.06 p.u. and $U_{P,\mathrm{stop}}$= 1.10 p.u. (Table 2).

**Table 2.** Base case without DER.

| Case | VSI | P | L-index | FVSI | U |
|---|---|---|---|---|---|
| Without DER | Bus 18 V=0.9038 | 210.9 kW | 0.1063 | 0.0298 stable | 0.9038 |
| 0 < λ ≤ 30%) | 0.9643 (λ = 0%) up 0.9781 (λ = 30%), 1, 41% up | | 0,1063 до 0,0842 | from 0.0298 to 0.0186 | 0.9038 to 0.9152 p.u. |
| 30% < λ ≤ 70% | Slow improvement to 55% 0.9891 | 145 kW | 0,0493 | | 0.9374 pu |
| 70% < λ ≤ 120% | Voltage monitoring | | | | 1 pu by λ ≈ 90% and up to 1.05 pu by λ ≈ 110% |
| λ > 120% | | Significan t reverse flows | The weakest bus before this becomes the bus with the highest voltage, and the stability margin is now limited by overvoltage | λ = 150%, all six buses have reduced stability | up 1.10 pu by λ ≈ 125%. |

The maximum load capacity (uniform load scaling to D = 0) is approximately 3.3 times the base load, resulting in a base VSM of approximately 67% at bus 18.

A parametric sweep from λ = 0% to 150% in 10% steps confirms the three-phase structure in all six indices. Results are presented for a concentrated DER deployment at bus 18 at cosφ=1. The distributed grids and uniform deployments show qualitatively identical phase transitions at shifted boundary values.

The phases are:

Phase 1 (0 < λ ≤ 30%). VSI at Bus 18 increases from 0.9643 (λ = 0%) to 0.9781 (λ = 30%), a 1.43% improvement. The L-index decreases from 0.1063 to 0.0842, FVSI_max decreases from 0.0298 to 0.0186, and the voltage at Bus 18 rises from 0.9038 to 0.9152 p.u. No reverse branch flows are observed.

Phase 2 (30% < λ ≤ 70%). VSI continues to improve, and the rate dVSI/dλ decreases. At λ = 50%, system losses reach their minimum (approximately 145 kW, a 31% reduction from the base case). VSI at Bus 18 reaches 0.9891 at λ = 70%. The L-index decreases to 0.0493. Voltage rises to 0.9374 p.u.

Phase 3 (70% < λ ≤ 120%). First sustained reverse flow appears at λ ≈ 80%. Voltage at Bus 18 exceeds 1.00 p.u. at λ ≈ 90% and reaches 1.05 p.u. at λ ≈ 110% under unity cos φ. The FVSI at branch 17→18 initially decreases to near zero (at λ ≈ 100%, when branch reactive flow reverses sign).

Phase 4 (λ > 120%). Significant reverse flows in branches upstream of Bus 18. Without Q(U) control, the voltage at Bus 18 exceeds 1.10 p.u. at λ ≈ 125%. The L-index begins increasing again, and the stability margin is now limited by overvoltage rather than undervoltage.

### 4.2 Impact of inverter control modes

Voltage control of Q(U) can improve the VSI of Bus 18 by 8–15% at high penetration (λ = 100–120%) compared to cos φ = 1. The improvement is greatest at λ = 110% because the VSI increases from 0.9932 (unit PF) to 1.0024 Q(U), reducing the destabilization of reactive power consumption at high voltage in (7). The improvement of FVSI$max$ is 12–18% because Q(U) modifies the reactive component of the flow in the branch, which enters linearly into FVSI (10). The penetration of the crossover λ* is shifted upwards by approximately 12% (from λ ≈ 90% to λ ≈ 102%).

When cos φ = 0.95, the reactive power is consumed, and the voltage at the load drops. The VSI improvement is 3–6% at λ = 100%, below Q(U), and the benefit is reversed at low penetration (Phases 1 and 2), where the additional reactive demand slightly degrades stability. The P(U) volt-watt limits the generation of active power P(U), which starts at λ ≈ 110% (bus voltage 18 exceeds 1.06 p.u.). The maximum bus voltage is limited to 1.10 p.u., regardless of λ, preventing entry into Phase 4. The energy yield loss is 7.2% at λ = 120% and 14.8% at λ = 150%. We added (U) + P(U) combined, which extends the hosting capacity to λ ≈ 130–140% while maintaining all voltages within ±10%. The VSI remains in its stable range. Impact of BESS

The collocated BESS should be 25% of the DER's nominal capacity. They significantly expand the hosting capacity. HC is defined as the maximum λ for which all bus voltages remain within [0.90, 1.10] under Q(U) control. For a concentrated 18-bus deployment, HC increases from 110% (without BESS) to 140% (with BESS). For a distributed deployment (18/25/33 buses), HC increases from 120% to 140% (+20 percentage points), and for a uniform deployment, HC increases from 130% to 150%.

The L-index trajectory confirms the mechanism that, without BESS, the $L_{System}$ exceeds the threshold of 0.75 at λ ≈ 120% (concentrated), while with BESS it remains below 0.75 until λ ≈ 145%. BESS charging in excess absorbs 25%, thereby leveling the voltage profile and reducing reverse current in the branches.

The stability-constrained OPF flow is solved with the help of equations (23)–(28) with $L_{max}$ = 0.75 and $VSI_{min}$corresponding to a 25% voltage stability margin. The sensitivity factors are recommended to be σ{P,18,18} = 0.0362 and σ{Q,18,18} = 0.0284. This means that active power generation on bus 18 has a stronger stabilizing effect than reactive power generation, due to the high R/X ratio of the low-voltage distribution branches.

With unconstrained OPF for stability, the flows are distributed approximately 8% less DER on bus 18 to the middle buses 8–12. This is the trade-off between the maximum VSI improvement on the weakest bus and the risk of overvoltage. The system losses increase by 3.1% (from 148 kW to 153 kW). This constrained stability guarantees VSM ≥ 25% on all buses while avoiding the disturbance on buses 17–18 for λ > 95%. The sensitivity-based linearization of constraints (27)–(28) converges within 4 iterations, demonstrating computational feasibility for planning studies.

## 5 Discussion

### 5.1 Practical implications

A structured methodology for planning DER integration in (ORS) for three phases is provided. In phases 1 and 2, DER integration has been found to have a clear positive impact. In the transition from phase 2 to 3, Q(U) control is recommended to be mandatory for stability. In Phase 3, BESS co-location becomes valuable for extending the stable operating range. Phase 4 operation requires comprehensive Volt-Var-Watt coordination and may require grid reinforcement. The proposed classification and measurement indices are shown to apply to IEEE 33-bus operation at 12.66 kV or to low-voltage (0.4 kV) grids according to the directives.

### 5.2 Limitations

This study uses balanced, equivalent modeling of single-phase systems. Future work is planned to extend the unbalanced three-phase analysis to test systems such as the IEEE 123-bus power supply. The static analysis framework does not capture the short-term voltage-stability phenomena associated with inverter-fault cycling or motor re-acceleration, which require dynamic simulation. The three-phase boundaries are topology dependent and must be recalculated for each specific grid.

## 6 Conclusion

This paper presents an analytical framework across three domains to characterize voltage stability in radial distribution grids with increasing DER penetration. For this purpose, a comparison of six classical voltage stability indices is conducted on the IEEE 33-bus test system.

For a comprehensive analysis, a taxonomy has been developed to separate the influence of the three phases based on the crossover index λ. They are low, moderate, high, and very high penetration, and based on them, the six indices are used for stability assessment. The goal is to limit the operation at ultra-high voltages, with $\lambda \approx 90\%$, for concentrated DER deployment on the weakest bus (Bus 18). Distributed and uniform deployment shifts this transition to $\lambda \approx 105\%$ and $\lambda \approx 115\%$, respectively.

Q(U) Volt-Var control provides a self-regulating stability advantage, improving VSI by 8–15% and FVSI by 12–18% at high penetration ($\lambda = 100$–$120\%$). Applying P(U) Volt-Watt limiting prevents overvoltage at the cost of a 7–15% loss in energy yield.

The collocated BESS increases hosting capacity by +30 percent for concentrated deployments and +20% for distributed deployments with Q(U) control.

Embedding the L-index as a hard inequality constraint in the OPF for DER deployment yields solutions with a guaranteed VSM ≥ 25%. This results in a redistribution of DER from the edges to the middle locations of the feeders, with a 3.1% change and no additional losses.

The closed-form sensitivity coefficients are $\sigma_P = 0.0362$ and $\sigma_Q = 0.0284$ at bus 18. This confirms that active power injection has a stronger stabilizing effect than reactive power in low-voltage grids. The proposed framework provides distribution system operators with an analytically sound, computationally efficient methodology for integrating DER while maintaining explicit voltage stability guarantees.

This study is financed by the European Union-NextGenerationEU, through the National 8 Recovery and Resilience Plan of the Republic of Bulgaria, project № BG-RRP2.013-0001.

## References

1. K. Gabrovska-Evstatieva, D. Trifonov, B. Evstatiev, A Review of the Key Factors Influencing the Performance of Photovoltaic Installations in an Urban Environment. Electricity, **6**(2):23 (2025). https://doi.org/10.3390/electricity6020023
2. V. Keseev, Comparison of Photovoltaic System Configurations with Different Azimuths and Tilts for Optimal Use of Available Installation Spaces. Eng, **7**(6), 268 (2026). https://doi.org/10.3390/eng7060268

3. W. Hao, M. Chen, D. Gan, Short-Term Voltage Stability Analysis and Enhancement Strategies for Power Systems With Photovoltaic Penetration, in IEEE Access, **12**, pp. 88728-88738 (2024), doi: 10.1109/ACCESS.2024.3408903
4. G. J. Lopez, J. W. González, I. A. Isaac, H. A. Cardona, O. H. Vasco, Voltage Stability Control Based on Angular Indexes from Stationary Analysis. Energies, **15**(19), 7255 (2022). https://doi.org/10.3390/en15197255
5. Y. Xu, Y. Chi, H. Yuan, Voltage Stability Indices, in Stability-Constrained Optimization for Modern Power System Operation and Planning, (2023) pp.293-310. doi: 10.1002/9781119848899.ch14
6. N. Mahmud, A. Zahedi, Review of control strategies for voltage regulation of the smart distribution network with high penetration of renewable distributed generation, Renewable and Sustainable Energy Reviews, **64** (2016) 582-595. https://doi.org/10.1016/j.rser.2016.06.030
7. J. Modarresi, E. Gholipour, A. Khodabakhshian, A comprehensive review of the voltage stability indices, Renewable and Sustainable Energy Reviews, **63** (2016) 1-12. https://doi.org/10.1016/j.rser.2016.05.010
8. B. B. Adetokun, C.M. Muriithi, J.O. Ojo, et al. Impact assessment of increasing renewable energy penetration on voltage instability tendencies of power system buses using a QV-based index.*Sci Rep* **13**, 9782 (2023). https://doi.org/10.1038/s41598-023-36843-5